Electronic Supplementary Material (ESI) for Journal of Materials Chemistry C.
This journal is © The Royal Society of Chemistry 2023

Supporting Information

Continuous Synthesis of All-inorganic Low-dimensional Bismuth-based Metal Halides $Cs_4MnBi_2Cl_{12}$ from Reversible Precursors Cs_3BiCl_6 and $Cs_3Bi_2Cl_9$ under Phase Engineering

Chunli Zhao[1], Yuan Gao[1,2*], Jianbei Qiu[1,2*]

[1]*Faculty of Material Science and Engineering, Kunming University of Science and Technology, Kunming 650093, China*

[2]*Key Lab. of Advanced Materials of Yunnan Province, Kunming 650093, China*

Corresponding Author

*E-mail: Yuan Gao (1251719335@qq.com); Jianbei Qiu (qiu@kust.edu.cn).

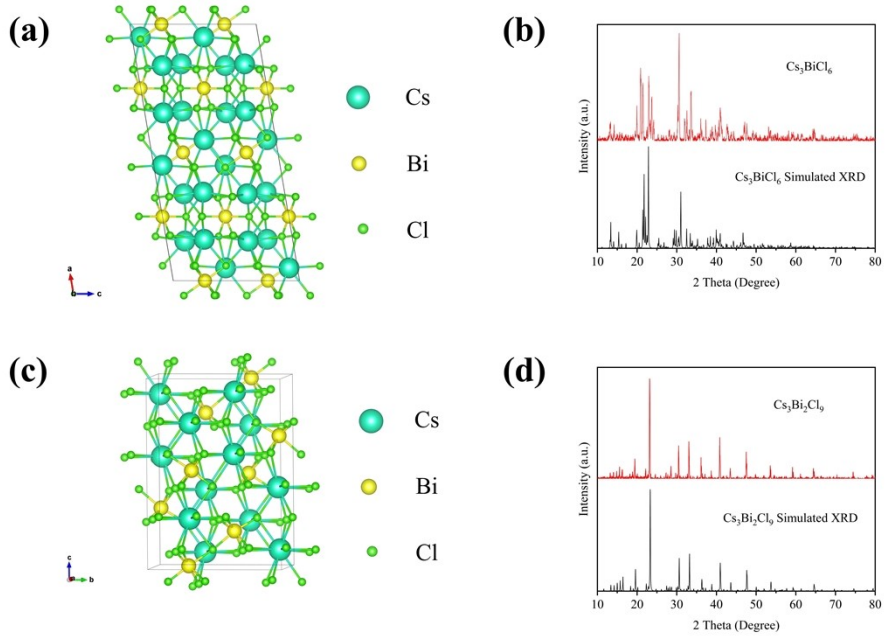

Figure S1. (a) Crystal structure of Cs_3BiCl_6. (b) XRD pattern of Cs_3BiCl_6 compared to the simulated pattern (PDF#22-0171). (c) Crystal structure of $Cs_3Bi_2Cl_9$. (d) XRD pattern of $Cs_3Bi_2Cl_9$ compared to the simulated pattern (PDF#70-0990).

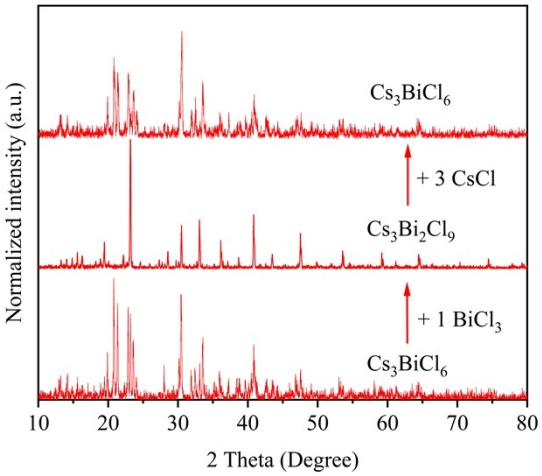

Figure S2. The XRD patterns of Cs_3BiCl_6 /$Cs_3Bi_2Cl_9$ and their continuous phase transformation after adding CsCl and $BiCl_3$, respectively.

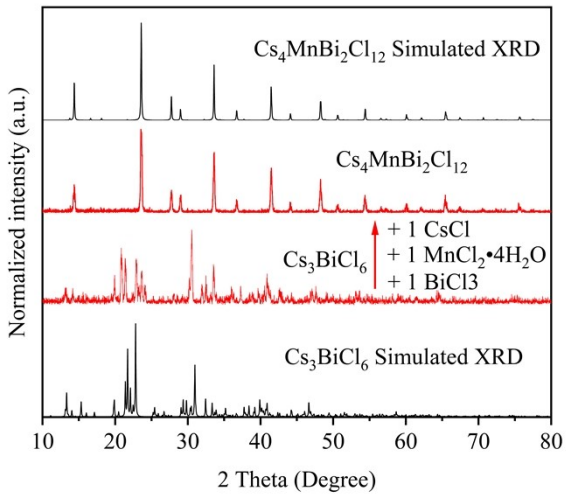

Figure S3. XRD patterns of Cs_3BiCl_6 as precursor, after adding $CsCl+MnCl_2.H_2O+BiCl_3$, and synthesized $Cs_4MnBi_2Cl_{12}$ phosphor.

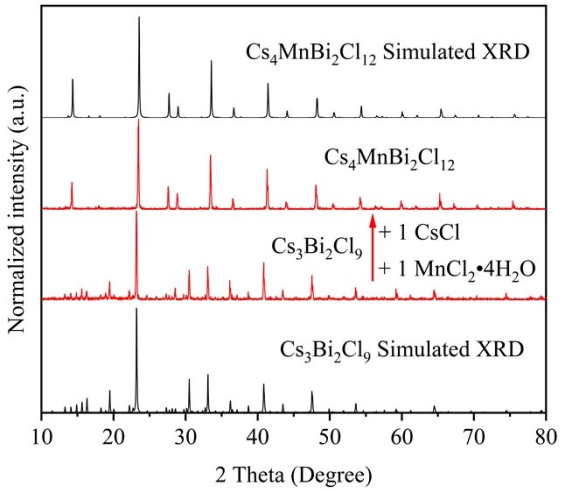

Figure S4. XRD patterns of $Cs_3Bi_2Cl_9$ as precursor, after adding $CsCl+MnCl_2.H_2O$, and synthesized $Cs_4MnBi_2Cl_{12}$ phosphor.

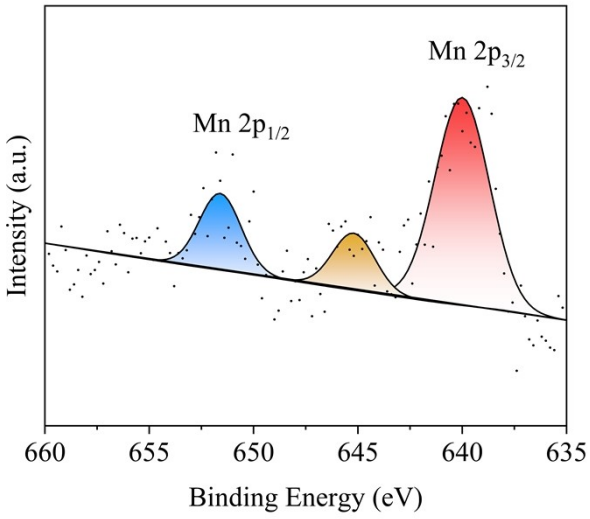

Figure S5. XPS spectra of Mn in $Cs_4MnBi_2Cl_{12}$ phosphor.

(a)

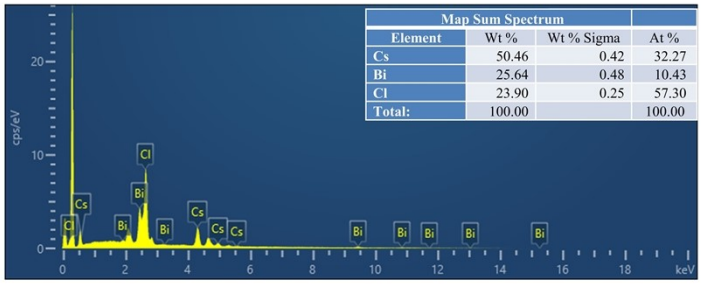

Map Sum Spectrum			
Element	Wt %	Wt % Sigma	At %
Cs	50.46	0.42	32.27
Bi	25.64	0.48	10.43
Cl	23.90	0.25	57.30
Total:	100.00		100.00

(b)

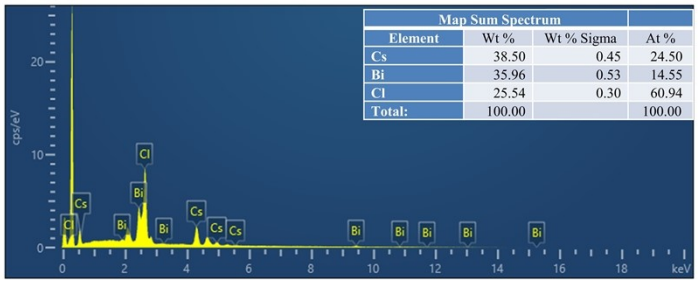

Map Sum Spectrum			
Element	Wt %	Wt % Sigma	At %
Cs	38.50	0.45	24.50
Bi	35.96	0.53	14.55
Cl	25.54	0.30	60.94
Total:	100.00		100.00

(c)

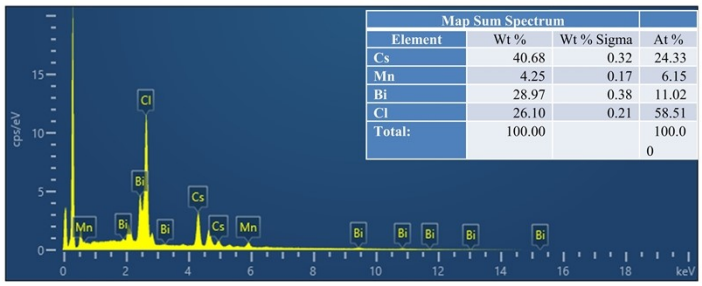

Map Sum Spectrum			
Element	Wt %	Wt % Sigma	At %
Cs	40.68	0.32	24.33
Mn	4.25	0.17	6.15
Bi	28.97	0.38	11.02
Cl	26.10	0.21	58.51
Total:	100.00		100.0 0

Figure S6. (a) The EDS spectrum of Cs_3BiCl_6. (b) The EDS spectrum of $Cs_3Bi_2Cl_9$. (c) The EDS spectrum of $Cs_4MnBi_2Cl_{12}$, respectively.

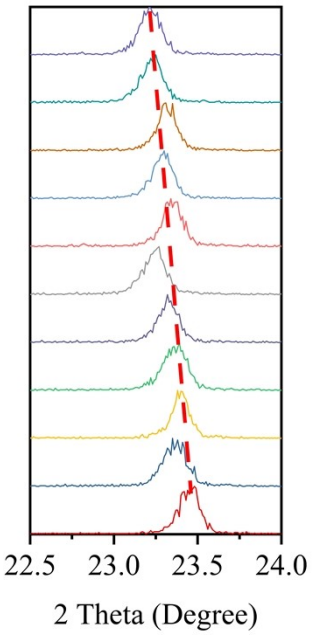

Figure S7. Selected diffraction peaks near 23.5° of $Cs_4Mn_{1-x}Cd_xBi_2Cl_{12}$ (x=0.0, 0.1, 0.2, 0.3, 0.4, 0.5, 0.6, 0.7, 0.8, 0.9, 1.0).

(a)

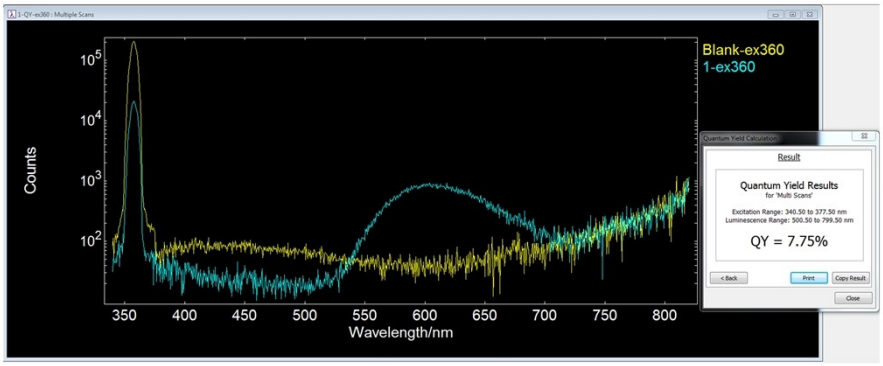

(b)

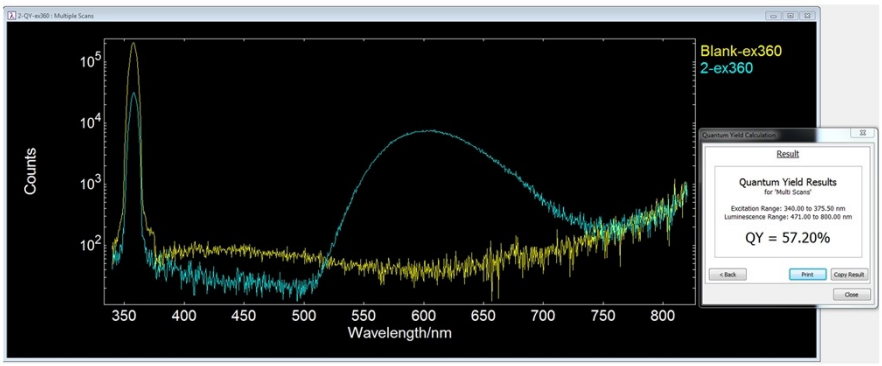

Figure S8. The measurement results of the optimal PLQY of (a) $Cs_4MnBi_2Cl_{12}$ and (b) $Cs_4Mn_{0.3}Cd_{0.7}Bi_2Cl_{12}$.

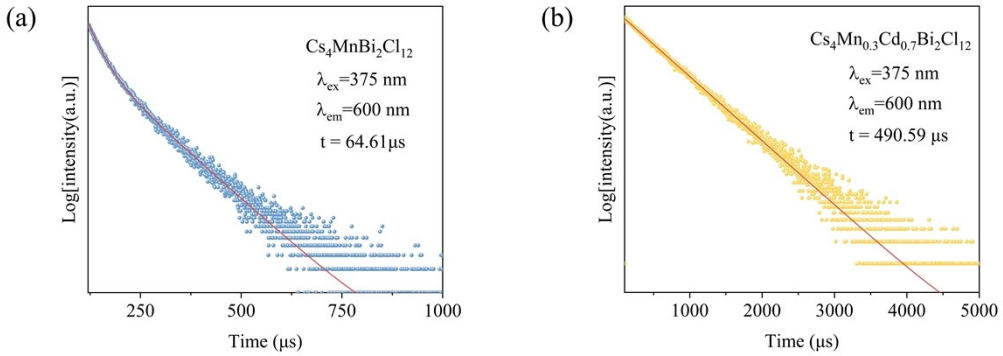

Figure S9. PL decay curves by monitoring Visible emission (λ_{em} = 950 nm) for the $Cs_4MnBi_2Cl_{12}$ and $Cs_4Mn_{0.3}Cd_{0.7}Bi_2Cl_{12}$ phosphor.

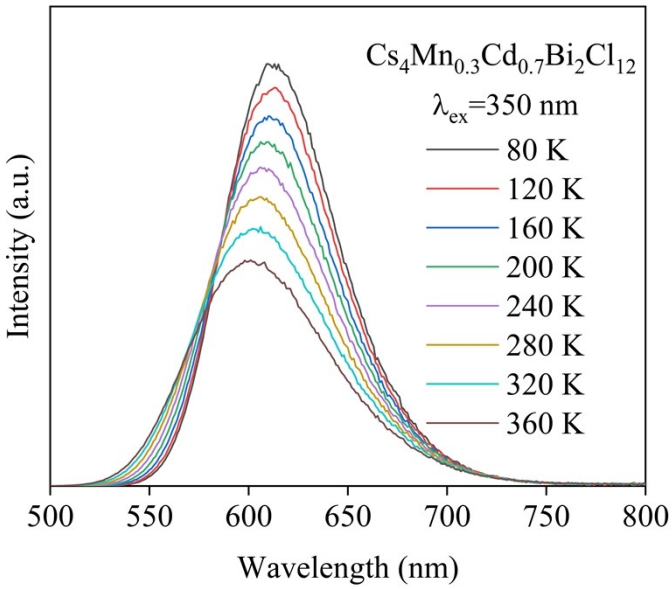

Figure S10. Temperature-dependent PL spectra for $Cs_4Mn_{0.3}Cd_{0.7}Bi_2Cl_{12}$.

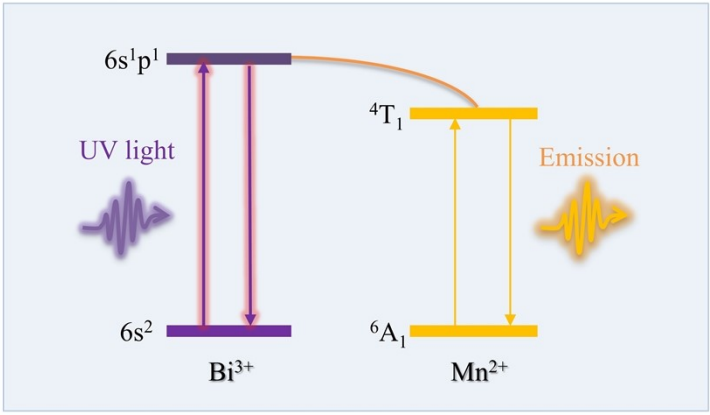

Figure S11. Schematic energy-level diagram illustrating the possible energy-transfer mechanism in $Cs_4Mn_{0.3}Cd_{0.7}Bi_2Cl_{12}$ sample under UV excitation.

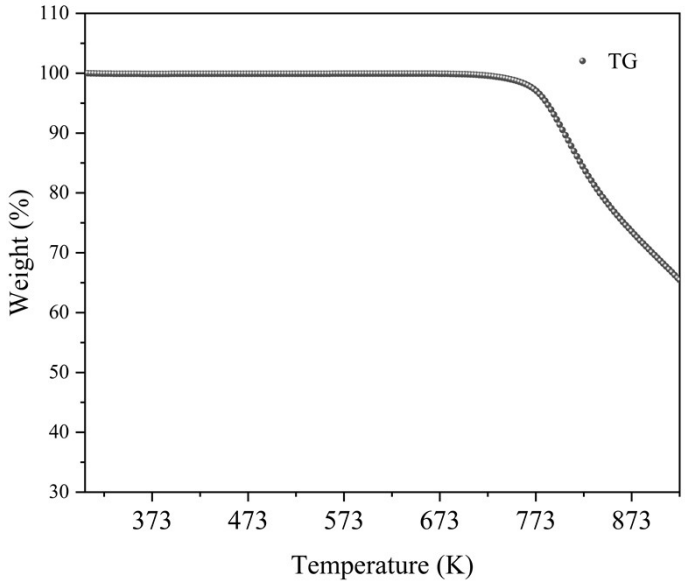

Figure S12. Thermogravimetric analysis graph of $Cs_4Mn_{0.3}Cd_{0.7}Bi_2Cl_{12}$.

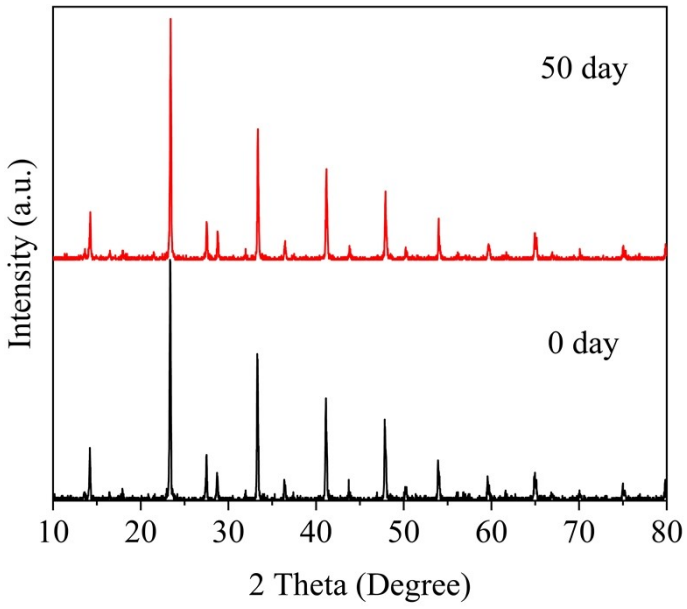

Figure S13. XRD patterns of the fresh $Cs_4Mn_{0.3}Cd_{0.7}Bi_2Cl_{12}$ sample and after exposing in air for 50 days.

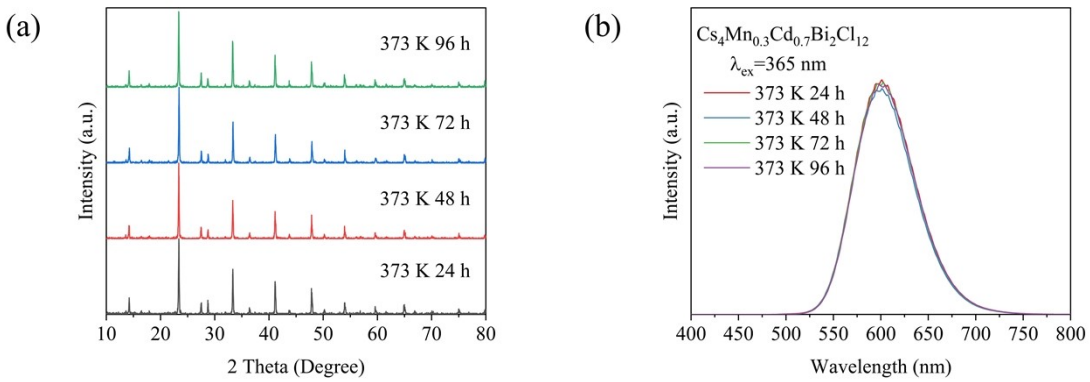

Figure S14. The (a) XRD patterns and (b) photoluminescence of thermal stability of the $Cs_4Mn_{0.3}Cd_{0.7}Bi_2Cl_{12}$ under 373 K heat.